Spatiotemporal Rogue Events in Optical Multiple Filamentation

Simon Birkholz and Erik T. J. Nibbering
Max-Born-Institut, Max-Born-Straße 2A, 12489 Berlin, Germany

Carsten Brée
Weierstrass Institute for Applied Analysis and Stochastics, Mohrenstraße 39, 10117 Berlin, Germany

Stefan Skupin
Max Planck Institute for the Physics of Complex Systems, 01187 Dresden, Germany, and Institute of Condensed Matter Theory and Optics, Friedrich Schiller University, 07743 Jena, Germany

Ayhan Demircan
Institut für Quantenoptik, Leibniz-Universität Hannover, Welfengarten 1, 30167 Hannover, Germany

Goëry Genty
Physics Department, Tampere University of Technology, 33101 Tampere, Finland

Günter Steinmeyer
Max-Born-Institut, Max-Born-Straße 2A, 12489 Berlin, Germany and Optoelectronics Research Centre, Tampere University of Technology, 33101 Tampere, Finland
(Received 8 July 2013; published 10 December 2013)

The transient appearance of bright spots in the beam profile of optical filaments formed in xenon is experimentally investigated. Fluence profiles are recorded with high-speed optical cameras at the kilohertz repetition rate of the laser source. A statistical analysis reveals a thresholdlike appearance of heavy-tailed fluence distributions together with the transition from single to multiple filamentation. The multifilament scenario exhibits near-exponential probability density functions, with extreme events exceeding the significant wave height by more than a factor of 10. The extreme events are isolated in space and in time. The macroscopic origin of these experimentally observed heavy-tail statistics is shown to be local refractive index variations inside the nonlinear medium, induced by multiphoton absorption and subsequent plasma thermalization. Microscopically, mergers between filament strings appear to play a decisive role in the observed rogue wave statistics.

DOI: 10.1103/PhysRevLett.111.243903 PACS numbers: 42.65.Sf, 52.38.Hb

Ocean rogue waves are rare events of extreme wave height [1]. While reports on such events have long been considered anecdotal and were received with skepticism, the first quantitative observation of the so-called Draupner wave [2] provided strong evidence for their existence. This pivotal observation stimulated research on extreme events in other areas of physics, in particular, in optical systems [3–5]. The appearance of rogue waves proved surprisingly ubiquitous, with a large number of wave-supporting physical systems exhibiting heavy-tail distributions of wave amplitudes or related quantities [6–9]. There is a particular rich variety of optical systems that exhibit rogue events [10], e.g., nonlinear optical fiber propagation. In this one-dimensional physical system, time series distributions of the filtered long wavelength components exhibit a pronounced heavy tail [3]. Similar extreme events have been observed in the temporal dynamics of single filaments [4]. In this Letter, we discuss a two-dimensional counterpart of the optical rogue waves previously observed in guided geometries. Similar to fiber optics, our system bears a dependence of propagation velocity on both wave number and wave amplitude, giving rise to linear optical diffraction and dispersion on one hand, and to the nonlinear optical Kerr effect on the other hand. These two major effects contribute to the formation of multiple filament strings [11–13] in the transverse plane of the beam. This two-dimensional localization appears similar to the formation of solitons in the one-dimensional system, yet also relies on clamping effects due to multiphoton ionization and resulting plasma formation.

Optical filaments are dynamic light structures with an intense core, which is able to propagate over extended distances, significantly larger than the usual diffraction length in the given medium. This effect allows maintaining a narrow beam size without any external guiding mechanism [12]. Filament formation is ruled by two counteracting nonlinear optical mechanisms, namely, self-focusing and plasma defocusing. Above the critical power $P_{\mathrm{crit}} \approx 0.15\lambda^2/n_0 n_2$ for self-focusing, a breakup of a spatially homogeneous beam profile into one or several

highly localized filament strings is observed [11,14,15]. Here, λ is the wavelength, and n_0 and n_2 are the linear and the nonlinear index of refraction, respectively. Assuming xenon gas at 2 atm pressure and $\lambda = 800$ nm as used in the experiments, we use $n_2 = 1.3 \times 10^{-18}\,\mathrm{cm}^2/\mathrm{W}$ [16], which sets a lower limit of $P_{\mathrm{crit}} \approx 800$ MW for the appearance of a single self-confined light filament, i.e., an optical power that can only be reached by pulsed laser sources. Multiple parallel filament strings are then expected to appear at several gigawatt input peak power [13]. Under these experimental conditions, we expect filament numbers $N < 12$ with the 5 mJ pulse energy of the Ti:sapphire laser used in the experiments. While single-shot transverse beam profiles of multiple filaments have frequently been measured, little record is available on the detailed shot-to-shot dynamics inside their beam profiles. Our experiments employed two different cameras to explore multifilament dynamics, namely, a 2048 pixel line scan camera that is capable of recording minute-long time series of a 0.3 mm cross-sectional wide slice of the beam profile at the full repetition rate and, alternatively, a megapixel area-scan camera that operates at a reduced frame rate of 100 Hz; see Fig. 1.

Theoretical predictions indicate the appearance of temporally and spatially isolated rogue waves in this two-dimensional system [17], however, with no experimental verification to date. From this theoretical work, one expects a similar noise amplification mechanism [18] as observed in the one-dimensional fiber case, with tiny fluctuations of the spatial input beam profiles being amplified to large-scale fluctuations at the output of the nonlinear medium. In the fiber system, this mechanism dramatically amplifies input fluctuations from quantum noise to a macroscopic level. Eventually, noise amplification also results in a loss of coherence between subsequent pulses [19]. Both these effects are expected to become stronger in a highly nonlinear medium, which suggests the use of nonlinear solid or liquid media for the straightforward observation of extreme events in filaments. We conducted a series of numerical simulations with random noise seeds and solved the nonlinear Schrödinger equation,

$$\partial_z \mathcal{E} = \frac{i}{2k_0}\nabla_\perp^2 \mathcal{E} + \frac{i\omega_0}{c} n_2 I \mathcal{E} - \frac{i\omega_0}{2n_0 c \rho_c}\rho(I)\mathcal{E}; \qquad (1)$$

see the Supplemental Material for a detailed description and parameters [20]. The results of the simulations are shown in Fig. 2(a). These simulations support our conclusion and also indicate that a major fraction of the rogue events in the multifilament scenario appears due to mergers between individual filament strings; see Fig. 2(b).

Given the beneficial influence of high nonlinearity in both theoretical as well as numerical investigations, we conducted early experiments in a water cell, but could not observe any heavy tail in the fluence distribution recorded by the camera, despite apparent multifilamentation with a large number of individual filament strings. Replacing the water cell by a xenon cell, however, heavy-tail fluence distributions are readily observed in the multifilament regime whereas near-Gaussian distributions dominate for single filamentation; see Fig. 3. Compared to ocean rogue waves and the optical fiber rogue wave scenario, the heavy tail in the distribution appears to be extremely pronounced [21]. For ocean waves, the significant wave height [22] is defined as the average value of the one third part of the largest recorded wave heights. Waves exceeding the significant wave height by a factor of two are generally considered rogue waves [23]. Applying the same criterion to the recorded fluence distributions, we find a large number of events that exceed the significant fluence $F_{1/3}$ by a factor of 5, with single events even appearing at $F \approx 10F_{1/3}$.

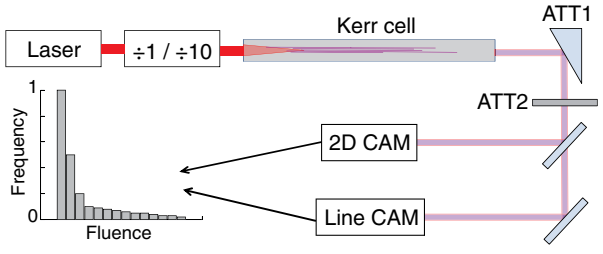

FIG. 1 (color online). Setup (schematic): Laser: pulsed Ti: sapphire chirped-pulse amplifier, delivering up to 5 mJ pulse energy at 1 kHz repetition rate. Pulse duration: 40 fs. $\div 1/\div 10$ selectable pulse division. Kerr cell: 1.5 m long cell filled with nonlinear refractive material (Xe, SF_6, water). ATT1: reflective attenuator. ATT2: absorptive attenuator. 2DCAM: Basler A504k, $12 \times 12\ \mu\mathrm{m}^2$ pixel size, 1280×1024 pixels, frame size 1.3 megapixels, $15.4 \times 12.3\ \mathrm{mm}^2$ detector size. Line CAM: Schäfter & Kirchhoff SK2048DDW, $13 \times 300\ \mu\mathrm{m}^2$ pixel size, 26.5 mm width, 2048 pixels. Inset: Example for resulting fluence histogram.

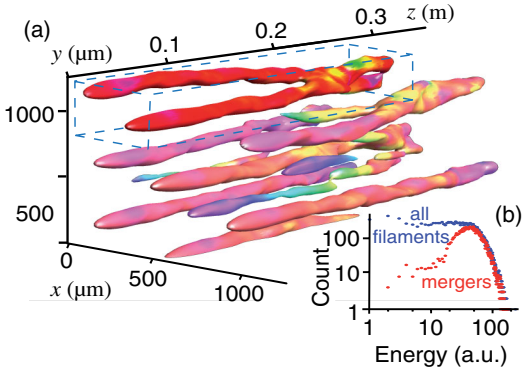

FIG. 2 (color online). Numerical simulations of the evolution of fluence distributions along the propagation coordinate z during multiple filamentation (for details see the Supplemental Material [20]). (a) Isofluence surfaces, with color coding showing relative phases. (b) Fluence statistics of filament strings, with separated merger events.

In order to further quantify the heavy-tail character, we also fitted Weibull probability density functions (PDF) to the measured data [24]:

$$\mathrm{PDF}_{\mathrm{W}}(F \parallel \alpha, \beta) = \frac{\beta}{\alpha}\left(\frac{F}{\alpha}\right)^{\beta-1} \exp\left[-\left(\frac{F}{\alpha}\right)^{\beta}\right], \quad (2)$$

where α and $\beta > 0$ are the scale and shape parameter of the distribution, respectively. Heavy-tail distributions are indicated by $\beta < 1$ whereas near-normal distributions exhibit large shape parameters of 10 and above. Our analysis indicates near-exponential distributions, with shape parameters below $\beta = 0.5$ for the case of multifilamentation [Fig. 3(c)]. In accordance with the above observations, the reported shape parameters are lower than those typically observed in oceanography [21] and nonlinear fiber optics [3], but similar near-exponential distributions have been reported for other physical systems [7,9]. We observe a very rapid transition from near-normal distributions characteristic for direct laser measurements and for single filamentation to heavy-tailed ones typical for multiple filamentation. This sharp transition is illustrated in Fig. 4, showing average fluence $\bar{F}$ and maximum fluence $F_{\max}$ vs position for different input powers ranging from 8 to 53 P_{crit} and for the linear case [Fig. 4(a)]. While increasing the input power beyond the threshold of multiple filamentation, the $\bar{F}$ and the $F_{\max}$ profiles increasingly separate. For the conditions in Fig. 4(c), corresponding to the appearance of two to three individual filaments strings, peak values may exceed the average fluence by factors larger than 10. We find single events that exceed $10F_{1/3}$ in a relatively small part of this beam profile. The most prominent region in this profile was specifically selected for the statistical analysis in Fig. 3(c); see highlighted area in Fig. 4(c). Looking at the significant fluence values in other parts of Fig. 4(c) and in Fig. 4(d), we find less extreme conditions, with fluences exceeding only about $5F_{1/3}$ despite of a more than doubled number of filament strings. Based on the criterion for ocean waves, there is still a large number of rogue events in the measured record. However, this trend also makes it clear that a large nonlinearity does not automatically lead to the most pronounced heavy-tail statistics in the multifilament system.

Despite the pronounced heavy-tail statistics within multifilament fluence dynamics, it is important to verify the isolated spatiotemporal character of the rogue events. Given the well-known spatial localized-wave character of individual filaments, it appears possible that the appearance of extreme events could be mocked by individual filaments crossing the detector array of the line scan camera. In other words, the observed shape parameter and significant wave height might merely measure the spatial distribution in the filament beam profiles, with a near-constant number of filament strings wandering around in this plane and occasionally causing high detector readings. The only safe way to rule out this somewhat disappointing explanation is a two-dimensional high-speed camera recording of a rogue event; see Fig. 5 and the Supplemental Material [20]. Specifically, Figs. 5(a)–5(e) display a sequence of 5 video frames recorded in the multifilament regime, with the appearance of one temporally and spatially isolated rogue event in Fig. 5(c).

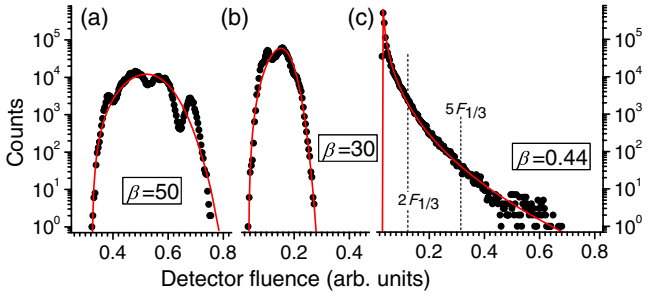

FIG. 3 (color online). Histogram analysis of 1 min line scan camera recordings (60 000 laser shots). Symbols represent the histogram of the accumulated 20 neighboring pixels in the most intense part of the beam profile. Line: Weibull fit. β defined according to Eq. (2). Detector fluence calibrated relative to the maximum limiting value. (a) Laser measured directly. $P \ll 8P_{\mathrm{crit}}$ (b) Single filamentation. $P = 8P_{\mathrm{crit}}$ (c) Multiple filamentation. $P = 19P_{\mathrm{crit}}$. Dashed lines indicate multiples of the significant fluence $F_{1/3}$. Data were taken out of the small marked part of the beam profile in Fig. 4(c).

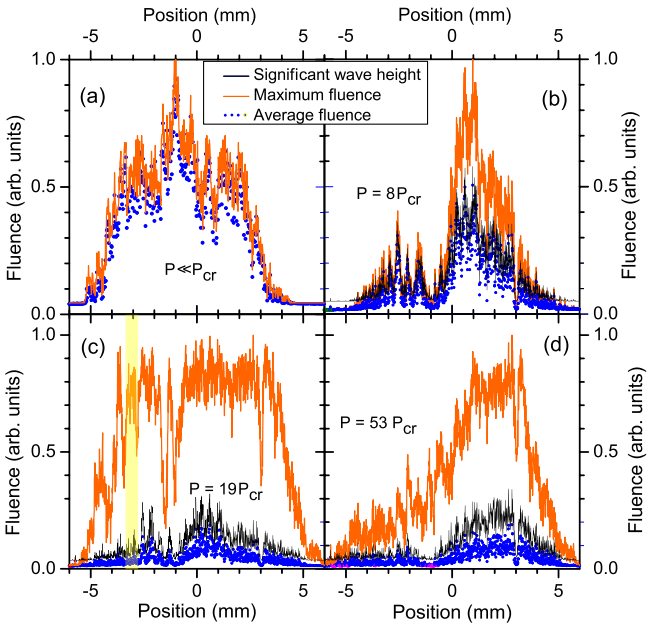

FIG. 4 (color online). Statistical analysis of 1 min line scan camera recording that includes 60 000 individual scans. Solid orange lines: maximum fluence $F_{\max}$. Blue dots: average fluence $\bar{F}$. Solid black lines: significant fluence $F_{1/3}$. (a) Input profile ($P \ll P_{\mathrm{cr}}$). (b) Profile after single filamentation ($P = 8P_{\mathrm{cr}}$). (c)–(d) Profile after multiple filamentation ($P = 19$ and $53P_{\mathrm{cr}}$). The region examined in the statistical analysis of Fig. 3(c) has been marked by a yellow semitransparent rectangle in (c). The sensitivity dip at 3 mm is an artifact of the camera.

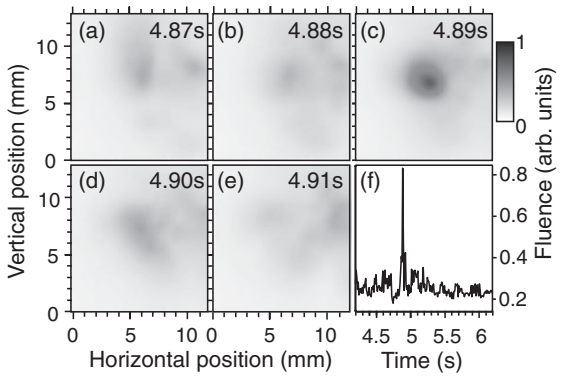

FIG. 5. (a)–(e) Sequence of 5 multifilament fluence profiles recorded with high-speed two-dimensional camera, with an extreme event appearing at 4.89 s after the start of recording. (f) Fluence observed at position (6 mm, 7 mm).

Figure 5(f) displays a longer record of the measured fluence at the location of this isolated rogue event, which somewhat resembles the Draupner event in oceanography [2]. These materials make it evident that the rogue events appear and disappear within the 10 ms time difference between two recorded video frames.

Notwithstanding the striking evidence for the appearance of extreme events in multifilaments, there is a number of peculiarities in our observations. First, rogue waves only appear in gaseous media with sufficiently high nonlinearity but not in water, a medium with about 100-fold higher Kerr coefficient. Moreover, we ran additional experiments in xenon with a synchronized chopper to reduce the laser repetition rate by a factor of 10. In spite of extended observation times, we could not record any indication for heavy-tail statistics in this situation, either. Moreover, to investigate the influence of input profile fluctuations on the observed dynamics, we conducted a Fourier analysis of the recorded line scan camera data, comparing input noise on the kHz pump laser with the dynamics in the far field of the Kerr cell; see Fig. 6(a). Other than for a laser oscillator, the noise of kHz amplifiers is mostly dominated by technical noise contributions rather than quantum noise. In the spectral representation, these contributions appear as narrow lines, rather than as white quantum noise signatures. In our case there is a dominant 300 Hz contribution, which is most likely being caused by the three-phase power supply of the laser itself. This particular frequency dominates beam pointing fluctuations, beam width changes, and all higher-order momenta extracted from the camera recording. In sharp contrast to the dominant narrow band contributions from the power supply, the fluence spectrum in the output plane is dominated by broadband *pink noise*, which neither seems to fit a technical noise origin nor an influence of quantum noise. In fact, the observed rogue wave dynamics appears to be completely unrelated to a noise-amplification process induced by input beam fluctuations.

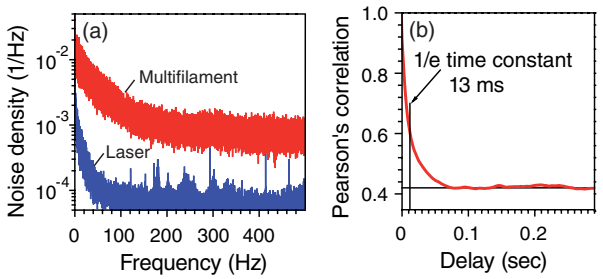

FIG. 6 (color online). (a) Fourier transform of line scan camera time series recorded directly at the laser output and after the Kerr cell for the case of multifilamentation. Sampling limit is 500 Hz. (b) Temporal correlation between individual line scan camera frames as a function of temporal delay between recordings in the multifilamentation regime.

Naturally, the above finding raises the question of an alternative explanation for the observed dynamics. To this end, it is instrumental to analyze the temporal correlation in the originally recorded data [Fig. 4]. Computing Pearson's correlation coefficient $\bar{r}(\Delta t)$ for all $F(t_1)$ and $F(t_2)$ at fixed $\Delta t = t_2 - t_1$ yields the temporal dependence shown in Fig. 6(b). In the case of observed rogue wave dynamics, this analysis indicates a temporal persistence of the dynamics of a few milliseconds, i.e., clearly above the delay between two laser pulses. We repeated this analysis for selected fluence spikes with $F > 5F_{1/3}$. This analysis confirms a temporal persistence of rogue events significantly beyond the pulse-to-pulse separation at kHz repetition rates, with some events lasting more than 100 ms. As this persistence cannot originate from the driver laser, the only possible explanation appears to be that information on the fluence pattern is stored by some physical mechanism inside the Kerr cell itself. To this end, one can either suspect atomic excitation or thermodynamic mechanisms. Given that xenon ions recombine within microseconds and given also that all known electronic excitations of xenon decay within about one microsecond [25,26], the observed millisecond persistence only leaves the thermodynamical explanation, i.e., lasting pressure or temperature effects that induce refractive index variations, similar to the mirage-like effects observed above a candle flame. These density variations are initially induced by local heating due to multiphoton absorption. Depending on the thermodynamic and mechanical properties of the medium, this local heating may give rise to turbulent natural convection inside the cell. Computing the local Grashof number $\mathrm{Gr}_{Q,y}$ [27,28], we find that about 1000 times higher powers are required to induce turbulent convection in water than in xenon. Assuming a $\approx 10\%$ laser power absorption in the cell and a $y = 10$ cm length scale, the Grashof number indicates an onset of turbulence in xenon. Reducing the average laser power by 10 as in the chopper experiments, however, we are unable to reach the transition zone between laminar and turbulent convection. Similar

conclusions are drawn from the Rayleigh number. We therefore conjecture that the appearance of rogue events in the multifilament system does not only depend on nonlinear optical properties as was suggested in [17]. Recently, the effect of long term gas dynamics has been discussed in the context of filamentation as gas density depressions [29]. These depressions and resulting refractive index variations have been discussed to persist for nearly a millisecond in argon and other air constituents, with an expected linear dependence of the lifetime function of thermal conductivity. Lifetimes of several milliseconds therefore appear plausible for xenon with its about 4 times lower heat conductivity, which also fits to the plume spectra discussed by Noto, Teramoto, and Nakajima for the transition between laminar and turbulent heat exchange [27].

In conclusion, we experimentally analyzed fluence patterns in laser-driven multifilamentation. Within the observed multifilament dynamics, rogue events have been detected that exceed the significant fluence by more than a factor of 10 and exhibit near-exponential probability distribution functions. Mergers between filament strings are identified as a possible microscopic driver mechanism for the observed rogue events, and atmospheric turbulence appears to play a decisive role in inducing these mergers. Our system allows the frequent observation of rogue events on a few-second time scale, implying rather modest observation requirements. Moreover, the system is two-dimensional as the ocean and filaments are accessible by small-scale numerical simulations. We therefore believe that multifilaments may prove an interesting test bed for further experimentation, which may lead to obtaining a more profound understanding of the intriguing yet often devastating physical phenomenon of extreme event statistics in physics.

We gratefully acknowledge fruitful discussions with H. M. Milchberg and J. M. Dudley. G. S. acknowledges support from the Academy of Finland (Project Grant No. 128844). A. D., S. B., and G. S. acknowledge partial support by DFG.

[1] L. Dysthe, H. E. Krogstad, and P. Müller, Annu. Rev. Fluid Mech. **40**, 287 (2008).
[2] S. Haver, in *Proceedings of Rogue Waves*, edited by M. Olagnon and M. Prevosto (Ifremer, Brest, France, 2004).
[3] D. R. Solli, C. Ropers, P. Koonath, and B. Jalali, Nature (London) **450**, 1054 (2007).
[4] J. Kasparian, P. Béjot, J.-P. Wolf, and J. M. Dudley, Opt. Express **17**, 12 070 (2009).
[5] F. T. Arecchi, U. Bortolozzo, A. Montina, and S. Residori, Phys. Rev. Lett. **106**, 153901 (2011).
[6] R. Höhmann, U. Kuhl, H.-J. Stöckmann, L. Kaplan, and E. J. Heller, Phys. Rev. Lett. **104**, 093901 (2010).
[7] A. N. Pisarchik, R. Jaimes-Reátegui, R. Sevilla-Escoboza, G. Huerta-Cuellar, and M. Taki, Phys. Rev. Lett. **107**, 274101 (2011).
[8] A. Chabchoub, N. P. Hoffmann, and N. Akhmediev, Phys. Rev. Lett. **106**, 204502 (2011).
[9] H. Xia, T. Maimbourg, H. Punzmann, and M. Shats, Phys. Rev. Lett. **109**, 114502 (2012).
[10] M. Onorato, S. Residori, U. Bortolozzo, A. Montinad, and F. T. Arecchi, Phys. Rep. **528**, 47 (2013).
[11] V. I. Bespalov and V. I. Talanov, Pis'ma Zh. Eksp. Teor. Fiz. **3**, 474 (1966) [JETP Lett. **3**, 307 (1966)].
[12] L. Bergé, S. Skupin, R. Nuter, J. Kasparian, and J.-P. Wolf, Rep. Prog. Phys. **70**, 1633 (2007).
[13] S. A. Hosseini, Q. Luo, B. Ferland, W. Liu, S. Chin, O. Kosareva, N. Panov, N. Aközbek, and V. Kandidov, Phys. Rev. A **70**, 033802 (2004).
[14] L. Bergé *et al.*, Phys. Rev. Lett. **92**, 225002 (2004).
[15] R. W. Boyd, *Nonlinear Optics* (Academic Press, San Diego, 1992), 2nd ed.
[16] C. Brée, A. Demircan, and G. Steinmeyer, Phys. Rev. A **85**, 033806 (2012).
[17] P. M. Lushnikov and N. Vladimirova, Opt. Lett. **35**, 1965 (2010).
[18] N. R. Newbury, B. R. Washburn, K. L. Corwin, and R. S. Windeler, Opt. Lett. **28**, 944 (2003).
[19] G. Genty, M. Surakka, J. Turunen, and A. T. Friberg, J. Opt. Soc. Am. B **28**, 2301 (2011).
[20] See Supplemental Material at http://link.aps.org/supplemental/10.1103/PhysRevLett.111.243903 for an animated version of Figs. 2 and 5 as well as for a detailed description of the numerical simulations.
[21] G. Muraleedharan, C. Lucas, C. G. Soares, N. U. Nair, and P. G. Kurup, Ocean Eng. **54**, 119 (2012).
[22] B. Kinsman, *Wind Waves: Their Generation and Propagation on the Ocean Surface* (Dover, Mineola, NY, 2002).
[23] V. Ruban *et al.*, Eur. Phys. J. Spec. Top. **185**, 5 (2010).
[24] W. Weibull, J. Appl. Mech. Trans. ASME **18**, 293 (1951).
[25] M. N. Shneider and R. B. Miles, Phys. Plasmas **19**, 083508 (2012).
[26] A. Kramida, Yu. Ralchenko, J. Reader, and NIST ASD Team, NIST Atomic Spectra Database (ver. 5.0), http://physics.nist.gov/asd [2013, June 5] (Natl. Inst. Standards and Technology, Gaithersburg, MD, 2012).
[27] K. Noto, K. Teramoto, and T. Nakajima, J. Thermophys. Heat Transfer **13**, 82 (1999).
[28] S. Grafsrønningen and A. Jensen, Int. J. Heat Mass Transfer **57**, 519 (2013).
[29] Y.-H. Cheng, J. K. Wahlstrand, N. Jhajj, and H. M. Milchberg, Opt. Express **21**, 4740 (2013).